Mathematical Foundations and Computational Techniques for Emerging Technologies
Volume 14: Special Issue: SVGASCA Palem: Mar-2026

International Journal of Science, Engineering and Technology
ISSN: 2348-4098, P-ISSN: 2395-4752
Ch. Janaiah, 2026, 14:Special

2-D Bio-Convective Nanofluid Flow Past a Stretching Sheet in Presence of Motile Microorganisms with Cattaneo-Christov Heat and Mass Flux

Ch. Janaiah[1], B. Saidi Reddy [2]

[1]Department of Mathematics, Government Degree College, Alair, Yadadri Bhuvanagiri (Dt), Telangana State, 508101, India.

[2]Department of Mathematics, K. R. R. Govt. Arts & Science College (A), Kodad, Suryapet (Dt), Telangana State, 508206, India.

Abstract- This research examines the two-dimensional flow of a continuous bio-convective magnetohydrodynamic (MHD) nanofluid. This flow is driven by a porous substance stretched across a sheet and by movable gyrotactic microorganisms. Mass fluxes and Cattaneo-Christov heat are among the physical variables examined in order to understand the system's flow dynamics. Finding out how different things influence microorganisms, concentration, speed, and temperature is our main goal. Discovering this kind of flow issue is necessary for controlling the movement of heat and liquids around a stretched sheet. A variety of bioengineering applications, including microfluidics, cooling systems, and bioreactors (including microbial fuel cells), may make use of this material. There were practical reasons for starting the investigation, and there were also scientific grounds. The nonlinear ordinary differential equations derived from the governing equations may be solved using the MATLAB bvp4c tool. The effects on velocity, concentration, temperature, and microbial growth may be shown graphically. Moreover, the impacts on the Motile density, Sherwood number, skin friction, and Nusselt number parameters are shown in a table. Because it addresses the concerns raised by Rashidi et al. [21], this study stands out. This study has some common ground with Rashidi et al. [21].

Keywords- Bio-convection; MHD; Cattaneo-Christov mass flux; Microorganisms; Stretching sheet; Porous medium; Cattaneo-Christov heat flux; Nanofluid;

I. INTRODUCTION

The fields of environmental science and biological engineering are making use of bioconvection, a relatively recent idea in non-Newtonian fluid dynamics. Bacteria and other biological particles' behavior in non-Newtonian fluids must be understood by biomedical medication delivery systems. Improved targeting and performance may be possible with user-defined fluid dynamics. Since bio-convection facilitates the transport of nutrients and waste products through engineered tissues, it is believed that it influences cell survival and proliferation. Researchers in the field of environmental

https://doi.org/10.5281/zenodo.19468102

International Journal of Science, Engineering and Technology
ISSN: 2348-4098, P-ISSN: 2395-4752
P. Ramulu, 2026, 14:Special

engineering are studying bio-convection in non-Newtonian flows with the hope of developing more efficient bioreactors and bio separation systems. Energy generation, pollution treatment, and pollutant removal are all part of this category.

New technology and a better understanding of the inner workings of complicated biological systems may result from applying bio-convection to the study of non-Newtonian fluid dynamics. Mandal and colleagues investigated bacterial movement in bioconvective nanofluid flows and the Arrhenius activation energy [1]. The numerical behavior of magnetic bioconvection nanofluid flow was investigated in the work of Shahid and colleagues [2]. This flow is distinct due to its Arrhenius dynamics and temperature-dependent viscosity. Research by Ahmad et al. [3] investigated the process by which gyrotactic bacteria generate bioconvection inside a nanofluid flow via a porous media. The effect of nanoparticles on the migration of gyrotactic bacteria was investigated by Muhammad et al.

within the context of a Darcy-Forchheimer magnetohydrodynamic flow et al. [4]. Researchers Irfan, Muhammad, et al. [5] investigated the bio-convection radiative heat transfer flow of MHD Carreau nanofluid using computer modeling. Investigating the thermosolutal Marangoni effect on bioconvection in a gyrotactic bacterial solution, Kairi et al. [6] used an angled stretched sheet. Li et al. [7] investigated bioconvection Casson nanofluid flow across a nonlinear surface where microorganisms are in motion. There are applications for this in bioprocessing temperature engineering. Puneeth et al. [8] considered bioconvection from a theoretical perspective by studying the temperature characteristics of a moving Ree-Eyring nanofluid on a stretched sheet. A non-Newtonian nanofluid's thermo-solutal Marangoni bioconvection was investigated by Roy et al. in a multilayer media [9]. The Buongiorno model was used by Basit et al. [10] to investigate the heat radiation and bioconvective nanofluid flow on a wavy cylinder.

Those who research thermal radiation are among those who are now interested in the Cattaneo-Christov model of thermal and mass transport. Consider the effects on flow via porous materials when using heat diffusion in industry. Higher temperatures may amplify the effects of radiation. Countless technological operations take place when temperatures are abnormally high. This kind of labor is typical in nuclear reactors, gas engines, and propulsion systems. Ayub et al. [11] investigated the activation energy in Walter-B nanofluid using Cattaneo-Christov double-diffusion. The specialists examined a number of aspects, including magnetohydrodynamics, thermal radiation, double stratification, thermal generation/absorption, and second-order chemical processes. Researchers under the direction of Saidi Reddy [12] examined the three-dimensional motion of nanofluids over an exponentially stretched sheet.

They made advantage of the several slip effects and magnetic fields that make up the dual Cattaneo-Christov diffusion effects. Jakeer et al. [13] examined the effects of a heated barrier's placement on the flow of a magneto-hybrid nanofluid inside a porous hollow that is driven by a lid using the Cattaneo-Christov heat flux system. The effects of nonlinear thermal radiation and Cattaneo-Christov heat flow on the magnetohydrodynamic properties of Maxwell nanofluids, including the Arrhenius activation energy, were investigated by Azam in his research [14]. In the flow of a Williamson nanofluid, Farooq et al. [15] investigated the Cattaneo-Christov model of heat and mass flux over a narrow, vertical cylinder. Included in the flow was heat radiation and bioconvection. Using the Cattaneo-Christov theory, researchers Nabwey et al. [16] investigated the transfer of thermal and solutal heat in second-order fluids. The impact of magnetized dissipative Soret and dufour on the thermally radiated flow of Casson fluid along a stretched cylinder was investigated by Basha [17] using Cattaneo-Christov heat and mass flux models. According to Khan et al. [18], a modified second-grade nanofluid was investigated for activation energy and nonlinear thermal radiation using Cattaneo-Christov equations.

International Journal of Science, Engineering and Technology
ISSN: 2348-4098, P-ISSN: 2395-4752
P. Ramulu, 2026, 14:Special

Thermostatic enhancement and the Cattaneo-Christov heat flow theory were investigated in a mixed nano Oldroyd-B rheological fluid by Haneef et al. [19], with mass transfer concerns taken into consideration. Mubaddel et al. examined the Sisko nanofluid's bioconvection radiative flow from two angles, measuring the total heat and mass fluxes [20].

This work aims to address the gaps left by Rashidi et al. [21], which was influenced by the literature described above, by including bioconvection flow, magnetic field, Cattaneo-Christov heat, and mass flow in porous surfaces. By providing novel insights into the transport of heat and fluids, the discipline is greatly improved by the intricate interplay of several components in this form. In this study, we regulate the mass and heat transport in the flow system by means of the Cattaneo-Christov flux model. Besides that, we examined temperaturephoresis, magnetic and Brownian motion effects, and flow on porous surfaces. The top equations were examined using MATLAB's "bvp4c" approach. Most of this work is devoted to the following areas of inquiry:

- In terms of heat and mass transport, how does the Cattaneo-Christov flow model fare?
- In the context of motion propagation, how do magnetic fields and porous media operate?
- When Brownian motion and thermophoresis are changed, how does it affect concentration and temperature patterns?

II. FLOW GOVERNING EQUATIONS

This research examines the effects of applying a magnetic field on a boundary layer of a two-dimensional, viscous, non-Newtonian nanofluid. A porous media is poured into a stretched sheet, and the fluid is allowed to flow through it. The nanofluid is solid because it does not obey Newton's laws. The effects of Brownian motion and thermophoresis on mobile microorganisms are also investigated in the research. The study's assumptions are shown in Figure 1, which shows the flow pattern:

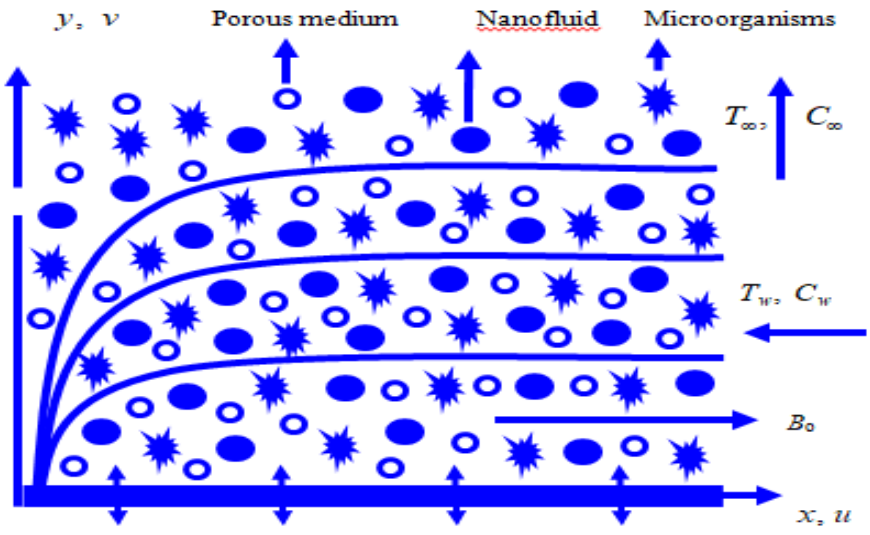

Fig. 1: Geometry representation of the nanofluid with swimming of microorganisms filled by porous medium

1. A power-law index is defined as the sheet's strain multiplied by the speed with the origin maintained in the same location, where n is a nonlinear stretching parameter, an is a constant, and x is the point perpendicular to the stress surface.
2. On a plate with a constant surface temperature ( ) and concentration ( ), a smooth fluid with a constant temperature ( ) and concentration ( ) is placed.

International Journal of Science, Engineering and Technology
ISSN: 2348-4098, P-ISSN: 2395-4752
P. Ramulu, 2026, 14:Special

3. As is common with MHD flow at low magnetic Reynolds numbers, a changing magnetic field B(x) is applied to the sheet surface when the magnetic field induced is modest.
4. Computations of energy concentration do not account for the Soret and Dufour effects.
5. In the concentration equation, neither the activation energy nor the consequences of chemical reactions are included.
6. Consequences of several slips are not considered.
7. Joule heating, fluid loss, and heat diffusion are not included into the energy computation.

According to the following equations, mass, velocity, energy, concentration, and microorganisms may be conserved if the criteria mentioned above hold:

Continuity Formula:

$$\frac{\partial u}{\partial x}+\frac{\partial v}{\partial y}=0, \tag{1}$$

Momentum Formula:

$$u\left(\frac{\partial u}{\partial x}\right)+v\left(\frac{\partial u}{\partial y}\right)=\nu\left(\frac{\partial^2 u}{\partial y^2}\right)-u\left(\frac{\sigma B_o^2}{\rho}\right)-u\left(\frac{\nu}{K^*}\right)..., \tag{2}$$

Thermal energy Equation:

$$\left(\left(u\frac{\partial T}{\partial x}\right)+\left(v\frac{\partial T}{\partial y}\right)\right)=\left(\alpha_m\times\nabla^2\times T\right)+\tau\left(\left(\frac{\partial C}{\partial y}\times\frac{\partial T}{\partial y}\times D_B\right)+\left(\left(\frac{\partial T}{\partial y}\right)^2\frac{D_T}{T_\infty}\right)\right)$$
$$-\omega_1\left(\left(u^2\frac{\partial^2 T}{\partial x^2}+v^2\frac{\partial^2 T}{\partial y^2}\right)+\left(\left(u\times\frac{\partial u}{\partial x}+v\times\frac{\partial u}{\partial y}\right)\times\frac{\partial T}{\partial x}\right)+\left(\left(u\times\frac{\partial v}{\partial x}+v\times\frac{\partial v}{\partial y}\right)\times\frac{\partial T}{\partial y}\right)+\left(2uv\frac{\partial^2 T}{\partial x\partial y}\right)\right), \tag{3}$$

Equation of species concentration:

$$\left(u\frac{\partial C}{\partial x}+v\frac{\partial C}{\partial y}\right)=D_B\left(\frac{\partial^2 C}{\partial y^2}\right)+\frac{D_T}{T_\infty}\left(\frac{\partial^2 T}{\partial y^2}\right)$$
$$-\omega_2\left(\left(\frac{\partial^2 C}{\partial x^2}\right)u^2+\left(\frac{\partial^2 C}{\partial y^2}\right)v^2+\left(u\frac{\partial u}{\partial x}+v\frac{\partial u}{\partial y}\right)\frac{\partial C}{\partial x}+\left(u\frac{\partial v}{\partial x}+v\frac{\partial v}{\partial y}\right)\frac{\partial C}{\partial y}+2\left(\frac{\partial^2 C}{\partial x\partial y}\right)uv\right)., \tag{4}$$

Equation of Microorganisms:

$$u\left(\frac{\partial \chi}{\partial x}\right)+v\left(\frac{\partial \chi}{\partial y}\right)=D_n\left(\frac{\partial^2 \chi}{\partial y^2}\right)-\frac{b^* W_c}{\left(C_w-C_\infty\right)}\frac{\partial}{\partial y}\left(\chi\frac{\partial C}{\partial y}\right)., \tag{5}$$

In the case of nano fluids, the flow boundary conditions

$$\left.\begin{aligned} &u=u_w\left(x\right)=ax^n..,C=C_w..,v=v_w\left(x\right)..,\chi=\chi_w..,\ T=T_w\ at\ y=0\\ &T\to T_\infty..,C\to C_\infty..,\chi\to\chi_\infty..,u\to 0..,\ v\to 0\ as\ y\to\infty \end{aligned}\right\} \tag{6}$$

International Journal of Science, Engineering and Technology
ISSN: 2348-4098, P-ISSN: 2395-4752
P. Ramulu, 2026, 14:Special

When $v_w(x)$ is negative, the velocity components at the stretching surface undergo a vertical shift; conversely, when $v_w(x)$ is positive, the velocity components are added. Rules (2), (3), (4), and (5) are solved by adding these proximity variables:

$$\left.\begin{aligned}\eta=\left\{y\sqrt{\frac{a(n+1)}{2\nu}}x^{\frac{n-1}{2}}\right\}..,v=-\left\{\sqrt{\frac{a\nu(n+1)}{2}}x^{\frac{n-1}{2}}\right\}\left\{f(\eta)+\left(\frac{n-1}{n+1}\right)\eta f'(\eta)\right\}..,\\ \theta(\eta)=\left(\frac{T-T_\infty}{T_w-T_\infty}\right)..,\phi(\eta)=\left(\frac{C-C_\infty}{C_w-C_\infty}\right)..,u=ax^n f'(\eta)..,N=\left(\frac{\chi-\chi_\infty}{\chi_w-\chi_\infty}\right)..,\end{aligned}\right\} \quad (7)$$

For the basic equations (2), (3), (4) and (5), Eq. (7) is used.

$$f'''+ff''-\left(\frac{2n}{n+1}\right)f'^2-Mf'-Kf'=0 \quad (8)$$

$$\theta''+\Pr f\theta'+\Pr Nb\theta'\phi'+\Pr Nt\theta'^2-\Pr Nb\omega\left\{f^2\theta''+ff'\theta'\right\}=0., \quad (9)$$

$$2Nb\phi''+NbLef\phi'+2Nt\theta''-2Nb\delta\left\{f^2\phi''+ff'\phi'\right\}=0 \quad (10)$$

$$N''+LbfN'-Pe\left(N'\phi'+\phi''\left(N+\Omega\right)\right)=0 \quad (11)$$

and the associated boundary conditions (5) become into

$$\left.\begin{aligned}f=f_w.,f'=1.,\theta=1.,\phi=1.,N=1at\,\eta=0\\ \phi\to0.,N\to0\,f'\to0.,\theta\to0\ as\ \eta\to\infty\end{aligned}\right\} \quad (12)$$

where the involved physical parameters are defined as

$$\left.\begin{aligned}\Pr=\frac{\nu}{\alpha}.,\ M=\frac{\sigma B_o^2x}{\rho a}.,\ Nb=\left(\frac{(\rho C)_p D_B(C_w-C_\infty)}{(\rho C)_f\nu}\right).,\ Nt=\left(\frac{(\rho C)_p D_T(T_w-T_\infty)}{(\rho C)_f\nu T_\infty}\right).,\\ f_w=-\frac{v_w(x)}{\sqrt{\frac{a\nu(n+1)}{2}}x^{\frac{n-1}{2}}}.,\ Lb=\frac{\nu}{D_n},\ Pe=\frac{b^*W_c}{D_n}.,\ \Omega=\frac{\chi_\infty}{\chi_w-\chi_\infty}.,\ K=\frac{2\nu}{K^*},\ Le=\frac{\nu}{D_B}.,\end{aligned}\right\} \quad (13)$$

These physical characteristics characterize the moist density coefficients, local Nusselt number, skin friction coefficient, and local Sherwood number:

$$Cf=\frac{\tau_w}{\rho U^2}\Rightarrow Cf=\left(\sqrt{\mathrm{Re}_x}\right)f''(0)., \quad (14)$$

$$Nu=\frac{Nu_x}{\sqrt{\mathrm{Re}_x}}=\left[-\left(\frac{xq_w}{T_w-T_\infty}\right)\left(\frac{\partial T}{\partial y}\right)\right]_{y=0}=-\left(\sqrt{\mathrm{Re}_x}\right)\theta'(0) \quad (15)$$

International Journal of Science, Engineering and Technology
ISSN: 2348-4098, P-ISSN: 2395-4752
P. Ramulu, 2026, 14:Special

$$Sh=\left(\frac{Sh_x}{\sqrt{\mathrm{Re}_x}}\right)=\left[-\left(\frac{xq_m}{C_w-C_\infty}\right)\left(\frac{\partial C}{\partial y}\right)\right]_{y=0}=\left(-\left(\sqrt{\mathrm{Re}_x}\right)\phi'(0)\right)., \quad (16)$$

$$Nh=\frac{xd_w}{D_n\left(\chi_w-\chi_\infty\right)}=-\kappa\left(\frac{\partial\chi}{\partial z}\right)_{z=0}\Rightarrow Nh=-\left(\sqrt{\mathrm{Re}_x}\right)N'(0) \quad (17)$$

" $\mathrm{Re}_x=\frac{Ux}{\nu}$ " is the area Reynolds number.

III. CALCULATIONS USING THE MATLAB BVP4C TOOL

Equations 8–12 reveal a collection of higher-order nonlinear ordinary differential equations (15). To solve these ODEs mathematically, one may utilize the bvp4c solution that is part of the MATLAB computer system. This "bvp4c" solution employs the three-stage Lobatto IIIA Runge-Kutta algorithm to rapidly discover excellent fourth-order integers. After that, we used our actual model to apply the bvp4c technique by following the steps below.

Step-1: An additional factor is introduced to the higher order nonlinear ODE system by equations (8)–(11).

$$\left.\begin{aligned} &y(5)=\theta',y(4)=\theta,y(1)=f,y(2)=f',y(3)=f'',\\ &y(7)=\phi.,\ y(8)=\phi'.,\ y(9)=N.,\ y(10)=N'. \end{aligned}\right\} \quad (18)$$

Step-2: After adding these extra parts to Equation 18, the higher-order nonlinear ODEs from Equations 8–11 are changed into a set of first-order nonlinear ODEs.

$$f'''=-y(1)y(3)+\left(\frac{2n}{n+1}\right)\left(y(2)\right)^2+My(2)+Ky(2)., \quad (19)$$

$$\theta''=-\Pr y(1)y(5)-\Pr Nby(5)y(8)-\Pr Nt\left(y(5)\right)^2+\Pr Nb\omega\left\{\left(y(1)\right)^2\theta''+y(1)y(2)y(5)\right\} \quad (20)$$

$$2Nb\phi''=-NbLey(1)y(8)-2Nt\theta''+2Nb\delta\left[\left(y(1)\right)^2\phi''+y(1)y(2)y(8)\right]., \quad (21)$$

$$N''=-Lbfy(10)+Pe\left(y(10)y(8)+\phi''\left(y(9)+\Omega\right)\right)., \quad (22)$$

Step-3: Applying the extra factors from Equation 18 to Equation 12's border conditions makes sense.

$$\left.\begin{aligned} &\left[y(1)\right]_p=f_w,\left[y(2)\right]_p=1.,\left[y(4)\right]_p=1.,\left[y(7)\right]_p=1.,\left[y(9)\right]_p=1.,\\ &\left[y(2)\right]_q\to 0,\left[y(4)\right]_q\to 0.,\left[y(7)\right]_q\to 0.,\left[y(9)\right]_q\to 0. \end{aligned}\right\} \quad (23)$$

For a given η = 0 value, the positions "p" and "q" indicate the sheet's zero position and its non-contact points. The location is η = 4in this investigation.

International Journal of Science, Engineering and Technology
ISSN: 2348-4098, P-ISSN: 2395-4752
P. Ramulu, 2026, 14:Special

Step-4: Apply the first-order nonlinear ODEs from (19) to (22), as well as the boundary conditions from (23), to the bvp4c solution.

Step-5: Achieve the 1st and 2nd results by running the bvp4c program with separate sets of initial values. Equation (12) determines if a set of initial estimates is valid by comparing them to the expected patterns of temperature and velocity. The process must be restarted with fresh initial assumptions if that does not work. A solid set of first forecasts requires several attempts.

IV. PROGRAM CODE VALIDATION

According to Rashidi et al. [21], the conclusions shown in Tables 1 and 2 are very congruent with the earlier numerical findings. These instances illustrate the absence of microbes, mass flows, Cattaneo-Christov heat, permeability, and magnetic field. Results in the same graphs created by Rashidi et al. [21] were also very close.

Table-1: Current temperature measurements are contrasted with those provided by Rashidi et al. [21].

η	Results of Rashidi et al. [21]	Present numerical results
0.0	1.00000000	1.00000000000
1.0	0.34838179	0.36056056109
2.0	0.12812649	0.14564056192
3.0	0.04815841	0.10665765824
4.0	0.01825518	0.20560725612
5.0	0.00694248	0.01064636098
6.0	0.00264353	0.00365760581

Table-2.: Checking the results provided by Rashidi et al. [21] against the most recent temperature data

η	Results of Rashidi et al. [21]	Present numerical results
0.0	1.00000000	1.00000000000
1.0	0.47170963	0.50579263509
2.0	0.13847506	0.15624583537
3.0	0.02894668	0.05554589345
4.0	0.00495102	0.00520145780
5.0	0.00077028	0.00105873508
6.0	0.00001546	0.00015792659

International Journal of Science, Engineering and Technology
ISSN: 2348-4098, P-ISSN: 2395-4752
P. Ramulu, 2026, 14:Special

V. RESULTS AND DISCUSSION

The goal of this research is to examine the influence of Cattaneo-Christov heat and mass fluxes on a non-Newtonian nanofluid that is stable, non-squishable, magneto-hydrodynamic, and electrically conductive. A novel property of the nanofluid is its ability to traverse a stretched sheet containing a porous media containing moving microorganisms. We are also investigating Brownian motion effects and suction/injection in addition to thermophoresis. The "bvp4c" approach is used in MATLAB for the purpose of solving the fundamental equations that govern the flow field. Several variables influence the microbial patterns, including velocity, temperature, quantity, and quality: M, K, fw, Pr, Nt, Nb, ü, Le, ε, Lb, Pe, and Ω, the microorganism difference parameter. Figures3,4,5, and 6 further provide the data for the mass transfer factors, skin friction, motile density, and warming rate.

The parameters that are taken into account are as follows: fw = 0.5 (suction) - 0.5 (injection), Pr = 0.71, Nb = 0.2, Nt = 0.3, ü = 0.2, Le = 0.5, δ = 0.1, Pe = 0.3, Lb = 0.2, and Ά = 0.1. For the research, these values were used. M, the measure of the magnetic field, may take on values between 0.2 and 0.8. The effects on the trajectories of speed are seen in Figure 2. As the value of the magnetic field increases, the velocity curves in this case decrease. When a magnetic field is applied to a fluid with electrical conductivity, an electromagnetic interaction takes place. As a result of the Lorentz force generated by this contact, the boundary layer fluid's velocity decreases. This is why the magnetic field component significantly impacts the flow patterns. Figure 3 displays the influence of the permeability measure on the velocity patterns for K = 0.1, 0.3, 0.5, and 0.7. In a typical situation, a higher permeability value indicates a faster flowing fluid. Reduced surface friction and easier fluid flow are characteristics of a porous material with a high permeability.

Figure 4 displays the altered velocity profiles in the domain of the stretched sheet boundary layer when the wall transpiration parameter is set to fw = -1.0, -0.5, 0.5, 1.0. Compared to when suction is present (fw = 0.5, 1.0), increased blowing (injection, fw = -1.0, -0.5) significantly accelerates the flow. The border layer becomes more adherent to the wall due to suction, which causes it to lose speed and slow down. A stream's temperature varies from a Prandtl value of 0.71 to 7.0, as seen in Figure 5. Conversely, when Pr increases, the stream's temperature differential decreases.

The momentum diffusivity rises in tandem with Pr and, in the long run, surpasses the temperature diffusivity. Heat is transferred by means of the rapidly flowing fluid. The result is a thinner boundary layer and quicker heat dissipation. Figures 6–9 illustrate the effects on the unitless temperature and nanoparticle concentration curves of the Brownian movement parameter (Nb = 0.3, 0.6, 0.8, 1.0) and the thermophoresis restriction (Nt = 0.5, 0.7, 0.9, 1.0). As the Brownian motion parameter (Nb) increases, the temperature profile rises but the volume concentration profile of nanoparticles falls. Our results show that the nanoparticles' temperature and volume are both affected by changes in the thermophoresis amount (Nt). The fluid rapidly escapes the stretched sheet due to the thermophoretic force generated by the temperature differential.

The fluid flows away from the developing surface as its temperature increases, as measured by the thermophoresis measure (Nt). Consequently, the hot limit layer thickness increases and the surface temperature slope decreases. The variation in concentration patterns at0.5,1.0,1.2, and 1.5 for the Lewis number is shown in Figure 10. The dimensionless Lewis number is shown by the temperature to mass diffusivity ratio. The volume percentage of nanoparticles decreases dramatically with increasing Le values. As seen in Figure 11, the distribution of temperatures is altered by the thermal relaxation time measure. As this value is increased, there is a noticeable decrease in temperature profiles due to the slower movement of heat. Figure 12 displays the time-dependent variation of the fluid's mass diffusion resistance. Lower concentration patterns are shown by increasing the mass relaxation time factors.

International Journal of Science, Engineering and Technology
ISSN: 2348-4098, P-ISSN: 2395-4752
P. Ramulu, 2026, 14:Special

Figure 13 shows that microbial patterns are impacted by the bioconvection Lewis number. The characteristics of microbes are significantly impacted by the Lewis number in bioconvection. As the bioconvection Lewis number increases, the quantity of bacteria in motion tends to decrease. This is due to the fact that a higher Lewis number indicates a lower mass diffusivity for microorganisms, which results in their displacement from specific regions and a reduction in their local density. The Peclet number (Pe) has a significant influence on the microorganism profiles that are present in bioconvection systems. Fig. 14 depicts this effect through the curves that it contains. As a general rule, the concentration or density of microbes tends to decrease as the number of Peclet number increases. The reason for this is that a larger Peclet number indicates that convection, which refers to the movement of large amounts of fluid, is superior than diffusion, which refers to the movement of particles in a random manner.

As a simplistic explanation, when convection is high, the movement of microorganisms removes them from the local area, which results in a reduction in the concentration of certain microorganisms. Figure 15 illustrates the effect of the microorganism difference parameter on microorganism profiles. The profiles of microorganisms in bioconvection are significantly influenced by the concentration gradient of microorganisms, which subsequently impacts their density and distribution. An elevation in the concentration gradient of microorganisms may lead to a decrease in the density of motile bacteria and an alteration in the thickness of their boundary layer. A number of technical parameters can influence the Skin-friction coefficient (Cf): n for the stretching sheet parameter, M for the magnetic field parameter, K for the permeability parameter, Pr for the Prandtl number, Nt for the thermophoresis parameter, Nb for the Brownian motion parameter, T for thermal relaxation, M for mass relaxation, Lb for bioconvection, and Peclet for biohydrodynamics. The Skin-friction coefficient is a measure of the heat transfer between two materials and increases in relation to the permeability, thermophoresis, and Brownian motion parameters. Contrarily, there is a discrepancy in the values of the following parameters: microorganism, Prandtl number, Thermal relaxation time, Mass relaxation time, Bioconvection Lewis number, and Stretching sheet parameter.

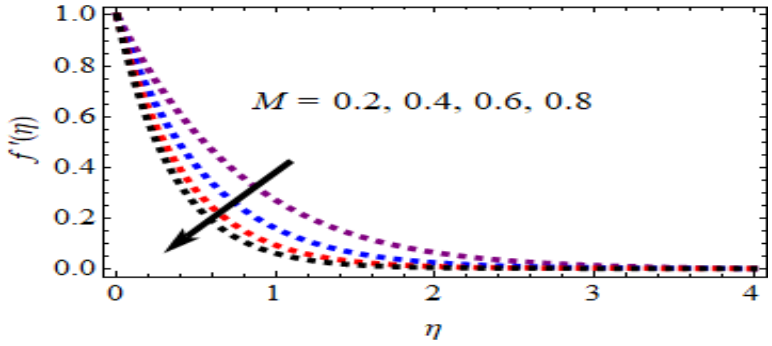

Fig. 2. Time series of velocities at various magnetic field parameters

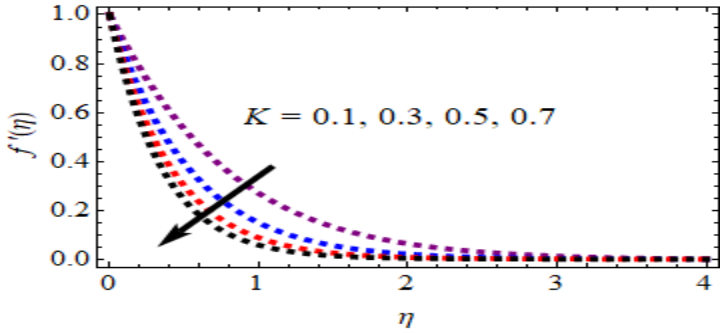

Fig. 3. Speed distributions for a range of permeability values

International Journal of Science, Engineering and Technology
ISSN: 2348-4098, P-ISSN: 2395-4752
P. Ramulu, 2026, 14:Special

In Table 4, we can see the rate of heat transfer coefficient expressed as a Nusselt number for various values of the Prandtl number (Pr), the thermophoresis parameter (Nt), the brownian motion parameter (Nb), and the thermal relaxation time parameter (ω). Increasing the brownian motion parameter (Nb) and the thermophoresis parameter (Nt) causes the rate of heat transfer coefficient to jump. The pattern contrary to what was expected emerges when both the Prandtl number (Pr) and the thermal relaxation time constant (ü) increase. In Table 5, we can see the effects on the rate of mass transfer coefficient, also known as the Sherwood number coefficient, of the following parameters: the Lewis number (Le), the Brownian motion parameter (Nb), the thermophoresis parameter (Nt), and the mass relaxation time parameter (ε).

This table shows that when the thermophoresis parameter (Nt) increases, the rate of mass transfer coefficient slowing down decreases, and vice versa as the Brownian motion parameter (Nb), the mass relaxation time parameter (ε), and the Lewis number (Le) increase. For a visual depiction of how the mobile density coefficient is affected by the microbe difference parameter (Ω), the Peclet number (Pe), and the Bioconvection Lewis number (Lb), refer to Table 6. The decrease in the mobile density coefficient is accompanied by greater values of the microbe difference parameter (Ω), Peclet number (Pe), and Bioconvection Lewis number (Lb).

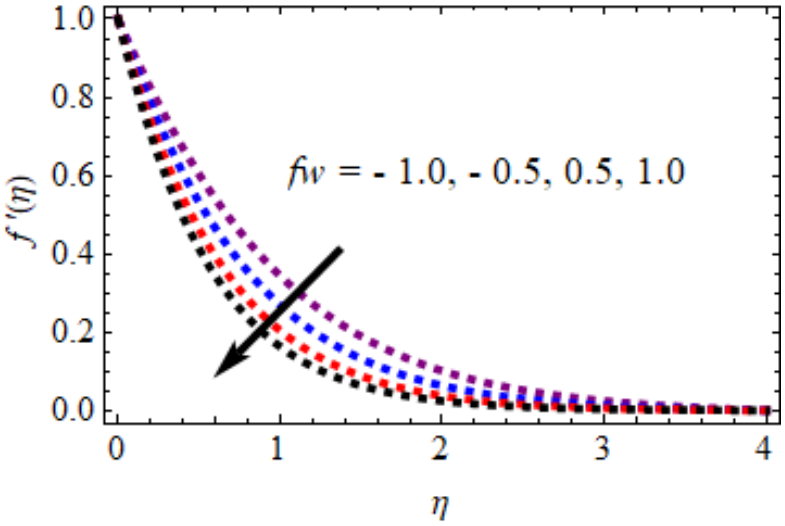

Fig. 4. Speed graphs for a range of Suction/Injection parameters

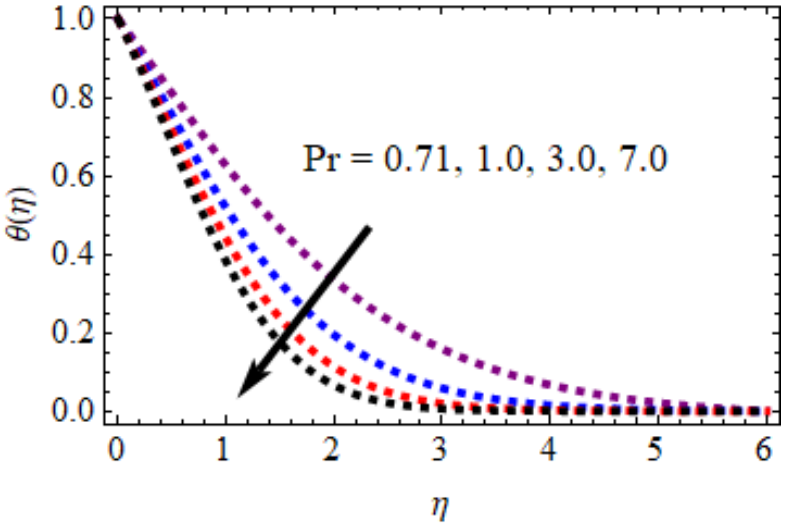

Fig. 5. Profiles of temperatures for various Prandtl numbers

International Journal of Science, Engineering and Technology
ISSN: 2348-4098, P-ISSN: 2395-4752
P. Ramulu, 2026, 14:Special

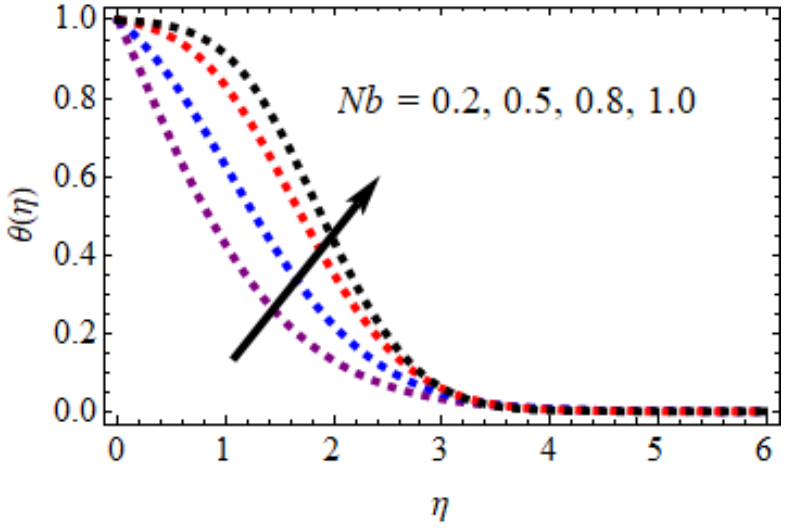

Fig. 6. Temperature silhouettes for different standards of Brownian motion parameter

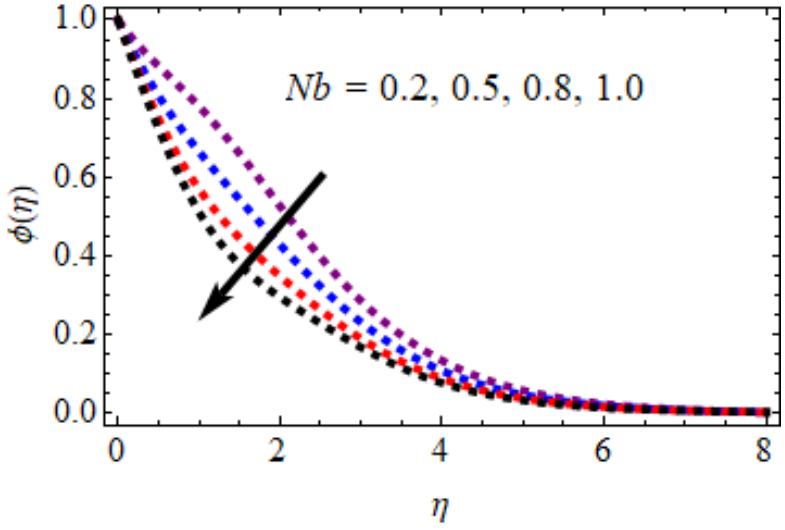

Fig. 7. Concentration distributions for a range of Brownian motion parameter values

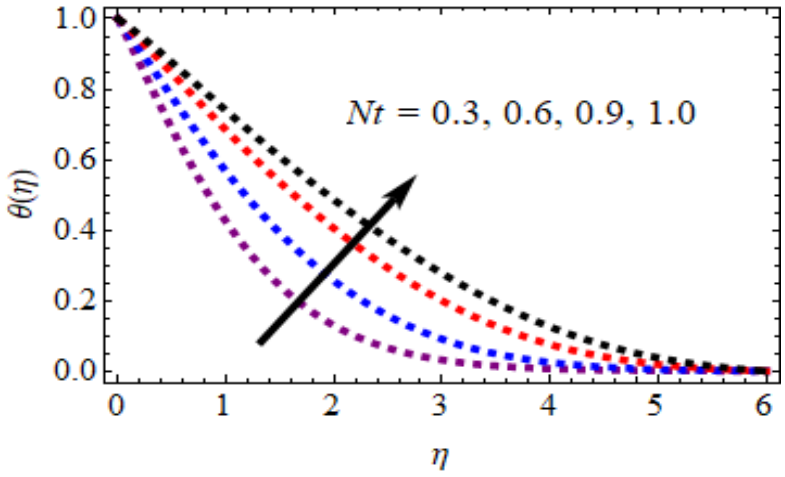

Fig. 8. Temperature silhouettes for a range of thermophoresis parameters

International Journal of Science, Engineering and Technology
ISSN: 2348-4098, P-ISSN: 2395-4752
P. Ramulu, 2026, 14:Special

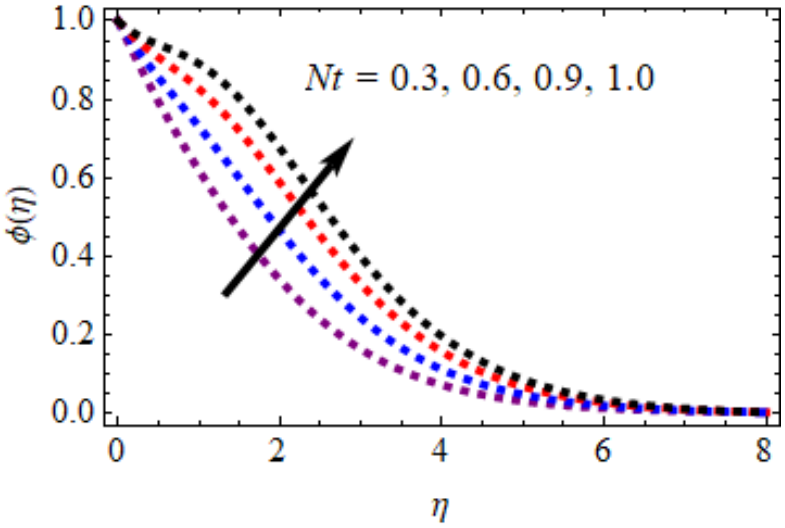

Fig. 9. Concentration silhouettes for different standards of Thermophoresis parameter

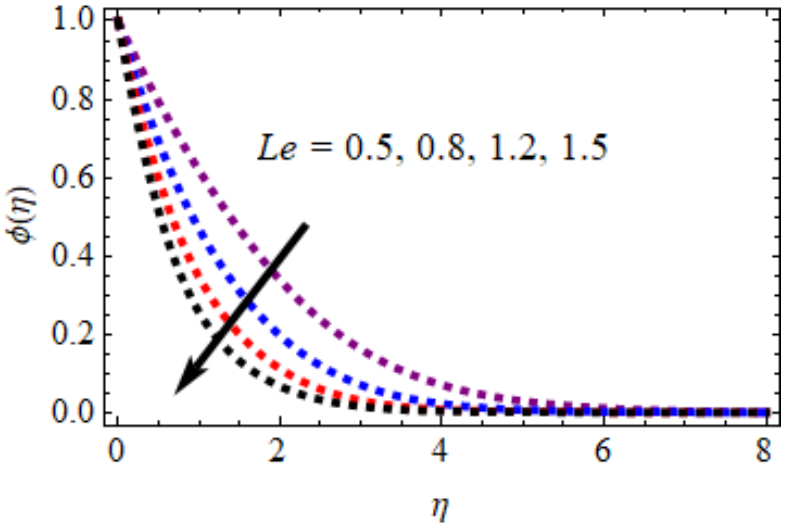

Fig. 10. Concentration distributions for a range of Lewis numbers

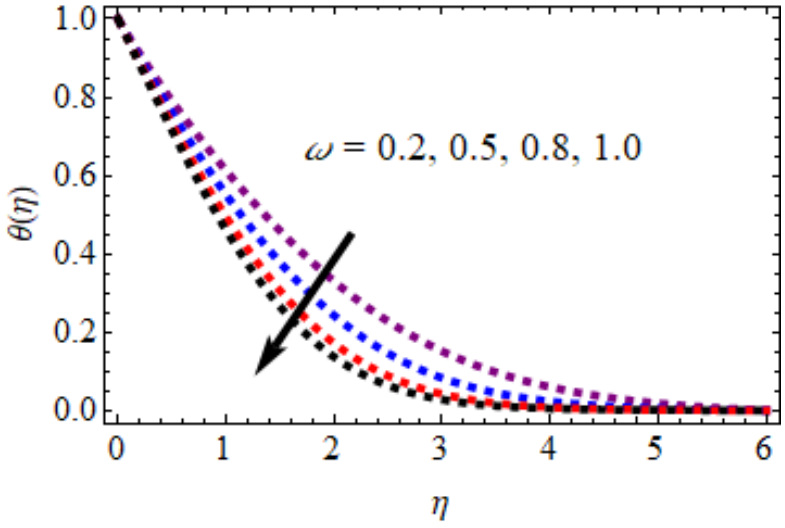

Fig. 11. Thermodynamic relaxation parameter temperature silhouettes for various values

International Journal of Science, Engineering and Technology
ISSN: 2348-4098, P-ISSN: 2395-4752
P. Ramulu, 2026, 14:Special

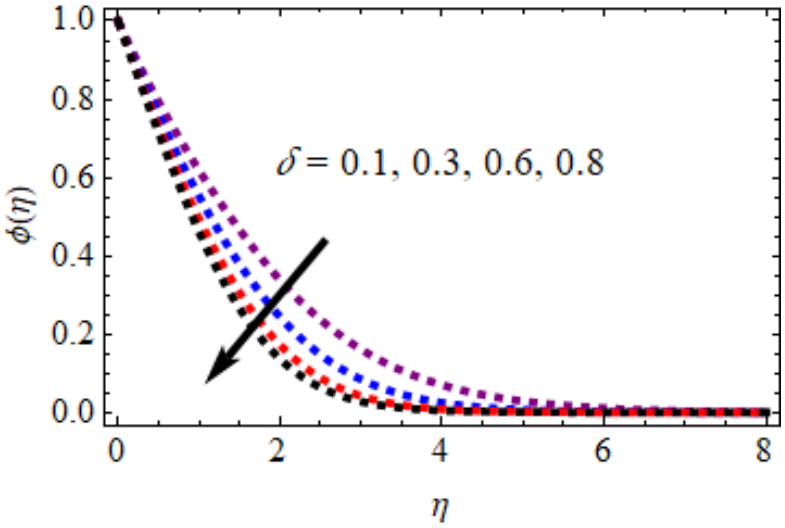

Fig. 12. Concentration silhouettes for different values of Mass relaxation parameter

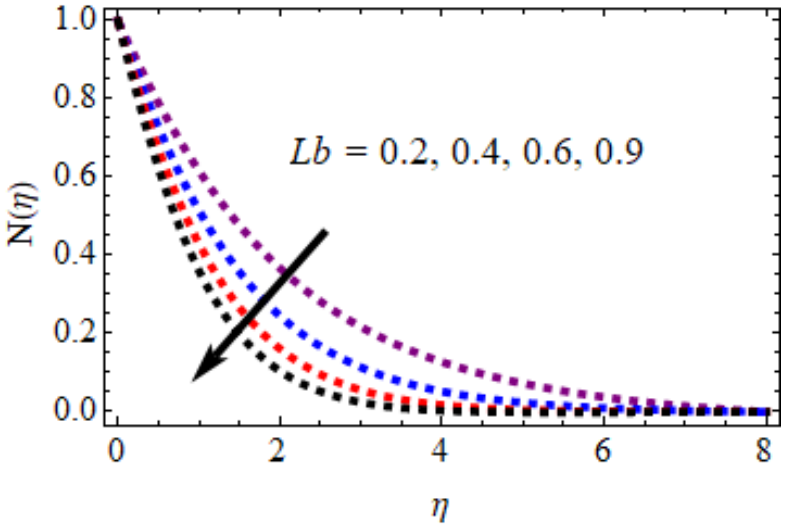

Fig. 13. Microbe silhouettes for various Bioconvection Lewis numbers

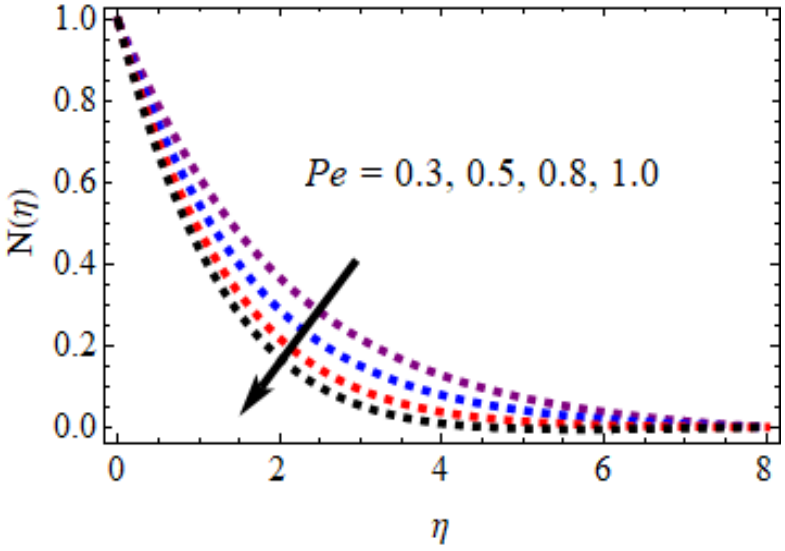

Fig. 14. Microbe profiles affected by pectin number.

International Journal of Science, Engineering and Technology
ISSN: 2348-4098, P-ISSN: 2395-4752
P. Ramulu, 2026, 14:Special

Table-3.: Estimated values of Cf.

M	K	f_w	n	Pr	Nb	Nt	Le	ω	δ	Lb	Pe	Ω	Cf
0.2	0.1	- 1.0	0.1	0.71	0.2	0.3	0.5	0.2	0.1	0.2	0.3	0.3	1.5767486963987
0.4													1.5355986352856
0.6													1.5054561064296
	0.3												1.5495982538567
	0.5												1.5299650926596
		- 0.5											1.6050631496039
		0.5											1.6205276258758
		1.0											1.6304807872870
			0.4										1.5945064377272
			0.6										1.6208376258402
				1.00									1.5307503640962
				3.00									1.5068570675870
					0.5								1.6067471465076
					0.8								1.6379364076463
						0.6							1.6149528635856
						0.9							1.6454082760874
							1.0						1.5548548485714
							1.2						1.5205723010734
								0.5					1.5423435825698
								0.8					1.5243956435987
									0.3				1.5464580745877
									0.6				1.5243597567579
										0.4			1.5176502657290
										0.6			1.4972028768726
											0.5		1.5375408278560
											0.8		1.5057745680265
												0.4	1.5264625396586
												0.7	1.5085648452573

Table-4.: Evaluated Nu values

Pr	Nb	Nt	ω	Nu
0.71	0.2	0.3	0.2	1.2365760986569
1.00				1.2046756204820
3.00				1.1842858272028
	0.5			1.2560276203640
	0.8			1.2750276507462
		0.6		1.2746585638633
		0.9		1.3056769036409
			0.5	1.1947659760972
			0.8	1.1646586545243

Table-5.: Evaluated Sh values

Nb	Nt	Le	δ	Sh
0.2	0.3	0.5	0.1	1.3546865284324
0.5				1.3187076503760
0.8				1.2746764390769
	0.6			1.3804976296291
	0.9			1.4160562650926
		1.0		1.3292649623956
		1.2		1.3066590269262
			0.3	1.3106576154692
			0.6	1.2956476723650

International Journal of Science, Engineering and Technology
ISSN: 2348-4098, P-ISSN: 2395-4752
P. Ramulu, 2026, 14:Special

Table-6.: Evaluated Nh values.

Lb	*Pe*	*Ω*	*Nh*
0.2	0.3	0.3	1.1187587153803
0.4			1.0756450265791
0.6			1.0423497354682
	0.5		1.0924656235314
	0.8		1.0651085610831
		0.4	1.0946269023492
		0.7	1.0642027835607

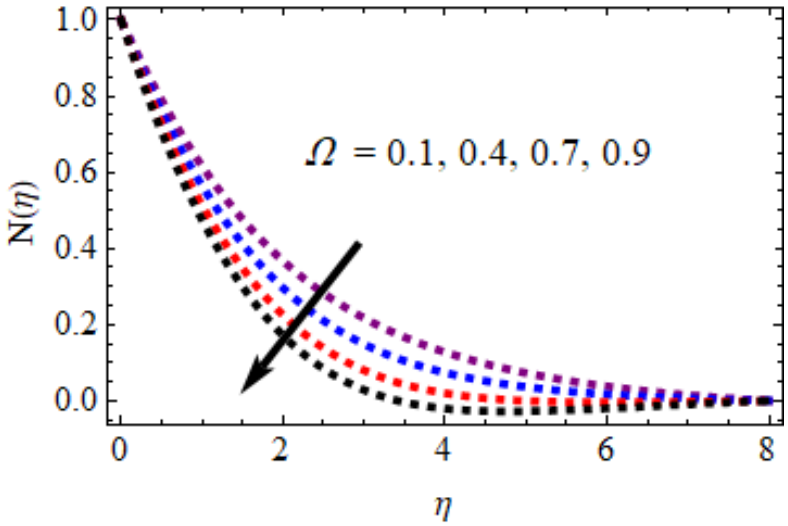

Fig. 15. Microorganism outlines for different values of Microorganism difference parameter

VI. CONCLUSIONS

A stretched porous sheet is continuously flooded with an electrically conducting nanofluid. The impact of Cattaneo-Christov heat and mass fluxes on this flow is examined in our work. In this experiment, we use Brownian motion effects, a magnetic field, and microorganisms that swim. For the primary MATLAB controlling equations, the "bvp4c" approach is used. The plots of microbe profiles, velocity, temperature, and concentration are made by modifying several engineering aspects once the computer solutions have been determined. Other numerical values provided in the table are the skin friction coefficient, motile density coefficient, local Sherwood, and Nusselt numbers. The key takeaways from this research are as follows:

- As the variables of magnetic field strength, porosity, and stretching sheet strength increase, the speed curves flatten out.
- The temperature profiles are proportional to the relative strengths of Brownian motion and thermophoresis. However, the converse occurs when the Prandtl number and thermal relaxation parameter increase in strength.
- With increasing mass relaxation, Lewis number, and Brownian motion parameters, the species concentration in the nanofluid falls. On the other hand, when the thermophoresis parameter increases, so does the species concentration.
- As the microbe difference factors, bioconvection Lewis number, and Peclet number increase, the microbe profiles shrink.
- The findings from the code validation are quite similar to those published by Rashidi et al. [21].

International Journal of Science, Engineering and Technology
ISSN: 2348-4098, P-ISSN: 2395-4752
P. Ramulu, 2026, 14:Special

REFERENCES

1. A. Mandal, H. Mondal, R. Tripathi, Activity of motile microorganism in bioconvective nanofluid flow with Arrhenius activation energy, Journal of Thermal Analysis and Calorimetry, 148 (17), (2023), pp. 9113-9130, 10.1007/s10973-023-12295-x.
2. A. Shahid, H. L. Huang, M. M. Bhatti, M. Marin, Numerical computation of magnetized bioconvection nanofluid flow with temperature-dependent viscosity and Arrhenius kinetic, Math. Comput. Simulat., 200 (2022 Oct 1), pp. 377-392, 10.1016/j.matcom.2022.04.032.
3. S. Ahmad, M. Ashraf, K. Ali, Bioconvection due to gyrotactic microbes in a nanofluid flow through a porous medium, Heliyon, 6 (12) (2020), Article e05832, 10.1016/j.heliyon.2020.e05832.
4. F. Muhammad, T. Tayebi, K. Ali, E. H. Malekshah, S. Ahmad, Interaction of nanoparticles with motile gyrotactic microorganisms in a Darcy-Forchheimer magnetohydrodynamic flow- A numerical study, Heliyon, 9 (2023), Article e17840.
5. M. Irfan, T. Muhammad, Numerical simulation of bio-convection radiative heat transport flow of MHD Carreau nanofluid, ZAMM Journal of Applied Mathematics and Mechanics, 104 (2024), Article e202300813numerical study, Heliyon, 9 (2023), Article e17840.
6. R. R. Kairi, S. Shaw, S. Roy, S. Raut, Thermosolutal marangoni impact on bioconvection in suspension of gyrotactic microorganisms over an inclined stretching sheet, Journal of Heat Transfer, 143 (2021), Article 031201.
7. Y. Li, A. Majeed, N. Ijaz, K. Barghout, M. R. Ali, T. Muhammad, Melting thermal transportation in bioconvection Casson nanofluid flow over a nonlinear surface with motile microorganism: Application in bioprocessing thermal engineering, Case Studies in Thermal Engineering, 49 (2023), Article 103285.
8. V. Puneeth, F. Ali, M. R. Khan, M. S. Anwar, N. A. Ahammad, Theoretical analysis of the thermal characteristics of Ree-Eyring nanofluid flowing past a stretching sheet due to bioconvection, Biomass Convertion Biorefinery, 14 (2024), pp. 8649-8660.
9. S. Roy, S. Raut, R. R. Kairi, Thermosolutal marangoni bioconvection of a non-Newtonian nanofluid in a stratified medium, Journal of Heat Transfer, 144 (2022), Article 093601.
10. M. A. Basit, M. Imran, R. Safdar, M. Tahir, M. R. Ali, A. S. Hendy, A. Alhushaybari, A. M. Alharthi, Thermally radiative bioconvective nanofluid flow on a wavy cylinder with buongiorno model: a sensitivity analysis using response surface methodology, Case Stud. Therm. Eng., 55 (2024 Mar 1), Article 104178, 10.1016/j.csite.2024.104178.
11. M. Ayub, M. Y. Malik, M. Ijaz, M. S. Alqarni, A. S. Alqahtani, Cattaneo-Christov double-diffusion model for viscoelastic nanofluid with activation energy and nonlinear thermal radiation, Multidiscip. Model. Mater. Struct., 16 (1) (2020), pp. 93-120, 10.1108/MMMS-03-2019-0046.
12. B. Saidi Reddy, Ch. Janaiah, R. Srinivasa Raju, Double Cattaneo-Christov diffusion effects on radiating three dimensional MHD Nanofluid flow past an exponentially stretching sheet with Multiple Slip effects, Journal of Radiation Research and Applied Sciences, Vol. 18, Issue 3, 2025, pp. 101800, https://doi.org/10.1016/j.jrras.2025.101800.
13. S. Jakeer, P. B. Reddy, A. M. Rashad, H. A. Nabwey, Impact of heated obstacle position on magneto-hybrid nanofluid flow in a lid-driven porous cavity with Cattaneo-Christov heat flux pattern, Alex. Eng. J., 60 (1) (2021), pp. 821-835, 10.1016/j.aej.2020.10.011.
14. M. Azam, Effects of Cattaneo-Christov heat flux and nonlinear thermal radiation on MHD Maxwell nanofluid with Arrhenius activation energy, Case Stud. Therm. Eng., 34 (2022), Article 102048, 10.1016/j.csite.2022.102048.
15. U. Farooq, H. Waqas, R. Makki, M. R. Ali, A. Alhushaybari, T. Muhammad, M. Imran, Computation of Cattaneo-Christov heat and mass flux model in Williamson nanofluid flow with bioconvection and thermal radiation through a vertical slender cylinder, Case Stud. Therm. Eng., 42 (2023), Article 102736, 10.1016/j.csite.2023.102736.

16. H. A. Nabwey, A. Abbas Khan, M. Ashraf, A. M. Rashad, Z. M. Abdelrahman, M. Abu Hawsah, Thermal and solutal heat transport investigations of second order fluid with the application of Cattaneo-Christov theory, PLoS One, 19 (7) (2024), e0304794, 10.1371/journal.pone.0304794.
17. H. Basha, Magnetized dissipative Soret and Dufour effects on thermally radiative Casson fluid flow over a stretching cylinder with Cattaneo-Christov heat and mass flux models, Waves Random Complex Media, 12 (2023), pp. 1-29.
18. S. U. Khan, I. Tlili, H. Waqas, M. Imran, Effects of nonlinear thermal radiation and activation energy on modified second-grade nanofluid with Cattaneo-Christov expressions, Journal of Thermal Analysis and Calorimetry, 143 (2021 Jan), pp. 1175-1186, 10.1007/s10973-020-09392-6.
19. M. Haneef, M. Nawaz, S. O. Alharbi, Y. Elmasry, Cattaneo-Christov heat flux theory and thermal enhancement in hybrid nano Oldroyd-B rheological fluid in the presence of mass transfer, Int. Commun. Heat Mass Tran., 126 (2021), Article 105344.
20. F. S. A. Mubaddel, U. Farooq, K. A. Khaled, S. Hussain, S. U. Khan, M. O. Aijaz, M. R. Gorji, H. Waqas, Double stratified analysis for bioconvection radiative flow of Sisko nanofluid with generalized heat/mass fluxes, Phys. Scripta, 96 (2021), Article 055004.
21. M. M. Rashidi, N. Freidoonimehr, A. Hosseini, O. Anwar Bég, T. K. Hung, Homotopy simulation of nanofluid dynamics from a non-linearly stretching isothermal permeable sheet with transpiration, Meccanica (2014) 49:469-482, DOI 10.1007/s11012-013-9805-9.